Núñez Valdez, M., Bruschini, E., Speziale, S., Bosi, F., Fregola, R. A., D'Ippolito, V., Andreozzi, G. B. (2018): Reexploring the cation ordering and magnetic cation substitution effects on the elastic anisotropy of aluminum spinels. - *Journal of Applied Physics*, *124*.

DOI: http://doi.org/10.1063/1.5050064

JOURNAL OF APPLIED PHYSICS **124**, 175901 (2018)

Reexploring the cation ordering and magnetic cation substitution effects on the elastic anisotropy of aluminum spinels

M. Núñez-Valdez,[1,a)] E. Bruschini,[2] S. Speziale,[1,b)] F. Bosi,[2] R. A. Fregola,[3] V. D'Ippolito,[2] and G. B. Andreozzi[2]
[1]*GFZ German Research Centre for Geosciences, Telegrafenberg, 14473 Potsdam, Germany*
[2]*Department of Earth Sciences, Sapienza University, Piazzale A. Moro 5, 00185 Rome, Italy*
[3]*Department of Earth and Geoenvironmental Sciences, University of Bari A. Moro, 70125 Bari, Italy*

(Received 27 July 2018; accepted 14 October 2018; published online 1 November 2018)

We study the effects of cation inversion x ($Mg \leftrightarrow Al$, with x representing the fraction of Mg and Al exchanged) and magnetic substitution ($Mn \rightarrow Mg$) on the elastic properties of the $MgAl_2O_4$ spinel system using density functional theory and Brillouin scattering techniques. Our computations show that cation inversion decreases the molar volume of spinel and produces a stiffening of C_{11} and a softening of C_{12}. Simulations and experiments agree within 2%. Density functional theory also captures the qualitative effect of $Mg \leftrightarrow Al$ on C_{44}, that is, an initial softening for inversion degree at $x < 0.125$ and stiffening at $x = 1$, with a disagreement of <4%. The Zener anisotropy factor A decreases with increasing degree of inversion. All these trends are preserved at high pressures. The substitution of Mn for Mg produces and increases the molar volume of spinel, and it is accompanied by the softening of both C_{11} and C_{44}, and the stiffening of C_{12} in good agreement with experimental results at ambient conditions. All these effects, which are qualitatively opposite to those of cation inversion, are enhanced at high pressures. The effect of $Mn \rightarrow Mg$ on the elastic anisotropy of spinel is, however, qualitatively similar to that of cation inversion, i.e., it causes a decrease in the Zener factor A. *Published by AIP Publishing.* https://doi.org/10.1063/1.5050064

I. INTRODUCTION

The spinel structure ($Fd\bar{3}m$, space group 227) is adopted by several materials that are important in industrial applications and geophysical models. In particular, $MgAl_2O_4$ spinel is widely used under harsh conditions such as in refractory ceramics,[1] covering in high-pressure discharge lamps,[2] and as radiation resistant material[3] due to its outstanding mechanical, thermal, dielectric, and chemical properties combined with its high optical/infrared transparency. In recent years, using the sintering method, high density $MgAl_2O_4$ spinel has been fabricated to broaden its applications.[4] Pure $MgAl_2O_4$ spinel is a natural crustal mineral and a major component of the spinel-structure phase present in the peridotitic rocks of the uppermost mantle (between ~5 and ~100 km depth or ≲3.5 GPa) of the Earth. In addition, $(Mg_{1-y}Fe_y)_2SiO_4$ ringwoodite, the most abundant mineral of the deep transition zone (between ~520 and 660 km depth or ~16 and 24 GPa), is isostructural to $MgAl_2O_4$ spinel. Figure 1 shows the conventional unit cell (u.c.) of spinel with eight formula units (f.u.) ($Z = 8$, 56 atoms). The spinel crystal structure is made of a nearly ideal cubic close-packed arrangement of oxygen (O^{2-}) anions with divalent cations (e.g., Mg^{2+} or Mn^{2+}) filling 1/8 of the tetrahedrally coordinated sites and aluminum cations (Al^{3+}) occupying 1/2 of the octahedrally coordinated sites. However, $MgAl_2O_4$ spinel usually shows some degree of inversion, x, between Mg^{2+} and Al^{3+}, written here as $(Mg_{1-x}Al_x)[Mg_xAl_{2-x}]O_4$, where parentheses ( ) represent tetrahedrally coordinated sites and brackets [ ] octahedrally coordinated sites. Spinel is called normal for $x = 0$ and inverse when $x = 1$. Materials with cubic symmetry are characterized by three independent elastic constants, C_{11}, C_{12}, and C_{44} (in Voigt notation), and the degree of inversion or disorder, in principle, has effects on their elastic anisotropy, which is given by the Zener's anisotropy factor[6]

$$A = \frac{2C_{44}}{C_{11} - C_{12}}. \quad (1)$$

It is important to understand to what extent A is affected by x, as variations in A can impact the performance of $MgAl_2O_4$ spinel in functional applications. In geophysics, recent discovery of natural ringwoodite with high degree of inversion[7] has revived interest in understanding the effect of cation inversion on the elastic properties of the whole family of spinel-structured minerals,[8,9] which can be critical to describe the acoustic velocity propagation in the Earth's upper mantle and deep transition zone.

Cation ordering in $MgAl_2O_4$ spinel has been studied experimentally and computationally using X-ray diffraction, ultrasonic interferometry, neutron scattering, and first-principles techniques. Agreement between experimental and modeling results, however, is still not completely satisfactory for single crystal elastic constants even at ambient conditions and $x = 0$. For example, using density functional theory (DFT),[10,11] Li *et al.*[9] found that $C_{12} < C_{44}$, while other computational works[12–14] and several experimental studies[15–17] have reported the opposite behavior. This apparent disagreement, therefore, leads to a somewhat uncertain elastic anisotropy at ambient conditions, high pressure, and as a function

[a)]Electronic mail: mari_nv@gfz-potsdam.de
[b)]Electronic mail: speziale@gfz-potsdam.de

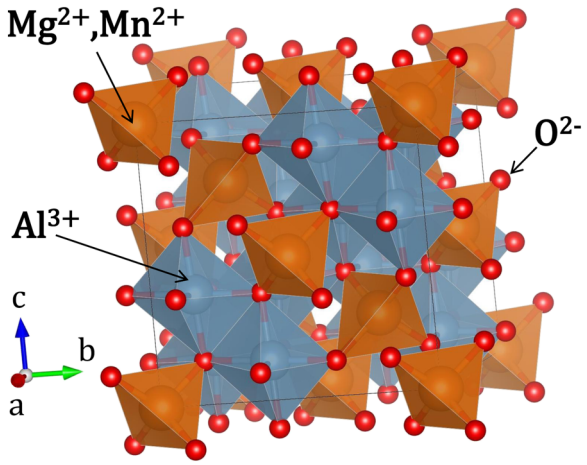

FIG. 1. $MgAl_2O_4$ spinel structure ($Fd\bar{3}m$, $Z = 8$, visualized using VESTA[5]) with origin fixed at $\bar{4}3m$, where Mg (or Mn), Al, and O occupy 8a (0, 0, 0), 16d (5/8, 5/8, 5/8), and 32e (u, u, u) Wyckoff positions, respectively.

of x. Thus, in the present work, in an effort to resolve or explain the possible differences, we revisit, experimentally and computationally, the structural and elastic properties of $(Mg_{1-x}Al_x)[Mg_xAl_{2-x}]O_4$ spinel as a function of pressure, P, and cation ordering, x, to re-asses its elastic anisotropy. Moreover, we extend our study to single crystal elastic constants and elastic anisotropy of $MnAl_2O_4$ galaxite as a function of P, reported here for the first time, as it has been suggested that the transition metal cation substitution, Mn → Mg, might have a similar effect on the elastic anisotropy to that of inversion, Mg ↔ Al.[18]

II. METHODS

A. Computational details

For our DFT calculations, we employed the projector-augmented wave (PAW) method[19,20] as implemented in the Vienna *ab initio* simulation package (VASP, version 5.4.4)[21–23] and installed in the supercomputer JURECA (Jülich Research on Exascale Cluster Architectures).[24] We used primarily the local density approximation (LDA),[25] but we also tested and compared results from the general gradient approximation (GGA) in the Perdew-Burke-Ernzerhof (PBE)[26] formulation. The plane wave expansions were performed up to a kinetic energy cutoff of 600 eV and used a Γ-centered grid with $(2\pi \times 0.032)$ Å^{-1} spacing for the reciprocal space sampling of our 56-atom cells. Convergence of our full structural optimizations (internal coordinates and lattice parameters) at any given pressure was assumed when the forces on each atom were smaller than 1 meV/Å and the total energy changes less than 10^{-8} eV. The PAW potentials with valence electrons $3s^2$ for Mg, $3p^6 3d^6 4s^1$ for Mn, $3s^2 3p^1$ for Al, and $2s^2 2p^4$ for O were employed, and for the calculation of the elastic tensor C_{ij}, we used the strain-stress relationship method as described in Ref. 27

$$\sigma_j = C_{ij}\epsilon_i, \tag{2}$$

where σ_j and ϵ_i represent the stress and strain tensors, respectively, and $i, j = 1,...,6$. We applied $\pm\epsilon$ strains of magnitude 1%, and considering the cubic symmetry of our systems, we took the set $\{\epsilon_1, \epsilon_4 + \epsilon_5 + \epsilon_6\}$ following the convention of Ref. 27. The treatment of cation inversion is conceptually simple but computationally tends to be expensive as the number of possible atomic configurations increases rapidly with the number of atoms and sites available. Here, we sample a finite number of configurations produced using the SOD (site-occupancy disorder) code,[28] which makes use of the crystal symmetry of the lattice to find the inequivalent configurations with fractional site occupancy. To find the structural and elastic properties of $MnAl_2O_4$, we added the Hubbard U correction in the Dudarev formulation.[29] While some studies determine the value of U following a self-consistent prescription,[30] here, we tested $U = 3$ and 4 eV but found $U = 4$ eV to agree better with the experimental C_{ij} results of $MnAl_2O_4$ at ambient conditions;[18] this U value has also been used in the modeling of other Mn compounds[31,32] with VASP. A value of $U = 2$ eV was recently reported[33] in the calculation of the zero pressure C_{ij} of $MnAl_2O_4$; however, the deviations with respect to the experimental data were larger than those given by our results (discussed below).

B. Experimental details

We have performed experimental studies of both the structure and elastic properties of four spinel single crystals by combining X-ray diffraction and Brillouin scattering measurements at ambient conditions. The samples were three synthetic $MgAl_2O_4$ spinels with different degrees of inversion and one natural spinel of almost end member composition. The three synthetic crystals were produced by the flux growth technique as described in Ref. 34. Then, they were separately heat-treated and equilibrated at 873 K for 50 days (sample sp3-600), at 1073 K for 7 days (sample sp3-800), and at 1473 K for 1 h (sample sp3-1050). Heating time needed to reach equilibrium at the three temperatures was calculated on the basis of spinel disorder kinetics.[35] The natural spinel (sample SP198B) is a gem-quality crystal from a marble unit in Pegu (Myammar) described in Ref. 36. The chemical composition of the synthetic crystals has been determined by microprobe analysis of six crystals belonging to the same batch of the ones investigated in this study. They are stoichiometric $MgAl_2O_4$ without any detectable content of other metals. The details of the measurements are reported in Ref. 34. The chemical composition of the natural spinel SP198B has also been determined by electron microprobe analysis. It has detectable Cr and Fe contents, traces of Zn and V, and it also presents excess Mg. Its structural formula is $(Mg_{0.852}Al_{0.136}Fe_{0.008}Zn_{0.004})$ $[Mg_{0.163}Al_{1.820}Cr_{0.013}V_{0.003}]$ O_4. Experimental details are described in Ref. 36. A structural study of the three synthetic spinels has been performed with a Bruker KAPPA APEX-II diffractometer equipped with a CCD area detector using MoK_α radiation. Data reduction and structural refinements were performed with the APEX2 software program by Bruker. The details of the experimental procedure are reported in Ref. 37. A crystal structure study of the natural spinel SP198B was performed by single-crystal X-ray diffraction with a 4-circle Siemens P-4 automated four-circle single-crystal diffractometer with a point detector using MoK_α radiation. Data reduction and

TABLE I. Ambient pressure unit-cell parameter a (Å), oxygen fractional coordinate u, density ρ (kg/m^3), elastic tensor C_{ij} (GPa), bulk modulus K (GPa), and shear moduli G_V and G_R (GPa) of $(Mg_{1-x}Al_x)[Mg_xAl_{2-x}]O_4$ spinel with different degrees of inversion x. Results from this work are labeled by *. MD[13] is a molecular dynamics work using a modified Coulomb potential to describe ionic interaction. Experimental (EXP) results are given by A: SP198B, B: sp3-600, C: sp3-800, D: sp3-1050. Experimental 1σ uncertainties on the last digits are reported in parentheses. We calculated the unit-cell parameter a for F using the density and chemical composition reported in Ref. 16.

x	a	u	ρ	C_{11}	C_{12}	C_{44}	K	G_V	G_R	Ref.
0	8.1577	0.38841	3481.05	258.7	144.83	142.79	182.79	108.45	89.07	GGA*
	8.0228	0.38834	3659.76	286.01	163.77	149.85	204.52	114.36	94.80	LDA*
	—	0.38759	—	274.2	151.8	159.4	192.6	120.1	97.1	LDA[a]
	—	—	—	292	162	161	193	123	101.2	LDA[b]
	—	—	—	405	212	186	276	150	136	MD[c]
	8.0330	0.38840	—	289	164	151	193	116	96.4	LDA[d]
0.125	8.0242	0.38480	3657.78	288.01	161.74	149.66	203.87	115.05	96.66	LDA*
	8.0217	0.38519	3661.25	286.72	161.16	148.75	203.08	114.36	96.10	LDA*
	8.0217	0.38688	3661.25	288.06	161.78	149.63	203.94	115.04	96.66	LDA*
	—	0.38689	—	280	147	150	191	100	117	LDA[a]
0.25	8.0220	0.38489	3660.96	288.61	159.29	148.42	202.60	114.91	97.74	LDA*
	8.0233	0.38488	3659.05	288.79	159.58	147.72	202.64	114.47	97.53	LDA*
	8.0223	0.38339	3660.40	289.30	159.55	148.58	202.79	115.10	98.00	LDA*
	8.0215	0.38538	3661.53	289.31	159.10	148.21	202.50	114.97	98.11	LDA*
	8.0223	0.38706	3660.40	288.43	159.71	148.02	202.62	114.56	97.38	LDA*
	8.0203	0.38658	3661.53	289.02	159.62	147.81	202.75	114.57	97.64	LDA*
	—	0.38638	—	281	145	150	190	101	117	LDA[a]
1	7.9823	0.37990	3715.89	333.97	154.31	152.27	214.17	127.30	119.08	LDA*
	7.9823	0.37940	3715.89	333.97	154.32	152.22	214.18	127.26	119.05	LDA*
	—	0.38194		319	145	158	203	119	130	LDA[a]
0.136(15)	8.0901(3)	0.38837(2)	3578.8(4)	282(1)	159(1)	154.3(5)	200(1)	96.2(6)	117.2(4)	EXP A*
0.198(15)	8.0871(2)	0.38764(3)	3573.2(3)	283(1)	157(1)	155(1)	199(1)	97.8(7)	118.2(7)	EXP B*
0.242(16)	8.0844(2)	0.38710(5)	3576.8(3)	282(4)	156(3)	154(1)	198(3)	97.6(22)	117.6(12)	EXP C*
0.286(16)	8.0830(2)	0.38654(4)	3578.7(3)	285(3)	154(1)	156(2)	197.7(19)	100.5(15)	119.8(14)	EXP D*
0.224(16)	8.0831(6)	0.38731(4)	3578.5(8)	282(1)	155(1)	154.0(2)	197.3(10)	98.1(6)	117.8(3)	EXP E[e]
0.02	8.0874	—	3576(3)	292.5(51)	168.9(53)	156.6(10)	210.1	97.1	118.7	EXP F[f]
0.23	8.0874	—	3576(3)	282.1(39)	155.4(41)	156.2(9)	197.6	98.5	119.1	EXP F[f]

[a]Reference 9.
[b]Reference 12.
[c]Reference 13.
[d]Reference 14.
[e]Reference 46.
[f]Reference 16.

structural refinements were performed with SHELXL-97 software.[38] The details of the experimental procedure and data analysis are analogous to those of Ref. 39. The degree of inversion was determined for all the crystals from the coordinates of the oxygen atoms using the linear calibration from Ref. 35. The resulting values are in systematic agreement with those based on fitting the cation distribution at tetrahedrally and octahedrally coordinated sites to both X-ray diffraction and microprobe results.[40] Brillouin scattering (inelastic scattering of light by acoustic phonons) has been measured at ambient conditions (295 $\pm$ 1 K; 1 atm) in the Brillouin scattering lab of the German Research Centre for Geosciences (GFZ) in Potsdam. The measurements were performed in forward symmetric scattering geometry.[41] We focused 80 mW of the 532.15 nm radiation of a Nd:YVO_4 laser on polished single-crystal sample platelets. The scattered radiation was analyzed by a Sandercock tandem Fabry-Perot (TFP) interferometer,[42] and the signal was detected by a photomultiplier tube. The sample platelets were prepared from slabs cut parallel to (111) or (110) growth faces. The facets were ground and polished with alumina sand-papers down to a final 1 μm grain-size. The two facets were parallel within 0.1°. The average width of the measured platelets ranges between 0.2 and 0.5 mm, and their thickness ranges between 0.05 and 0.2 mm. Brillouin scattering was collected in 17 to 36 directions in a range of 180° along the plane of the platelets. A total of 45 to 130 individual frequencies were measured for each sample platelet. Brillouin scattering was measured from 2 different platelets for each of the synthetic samples and from one platelet of the natural one. Measured Brillouin frequency shifts were converted to acoustic velocities as described in Ref. 41

$$v = \frac{\lambda_0 \omega_B}{2 \sin(\theta_e/2)}, \tag{3}$$

where v is the acoustic velocity, λ_0 is the wavelength of the incident laser, ω_B is the Brillouin frequency shift, and θ_e is the external scattering angle, that is, the angle between the incident and the scattered beam outside the sample. The sets

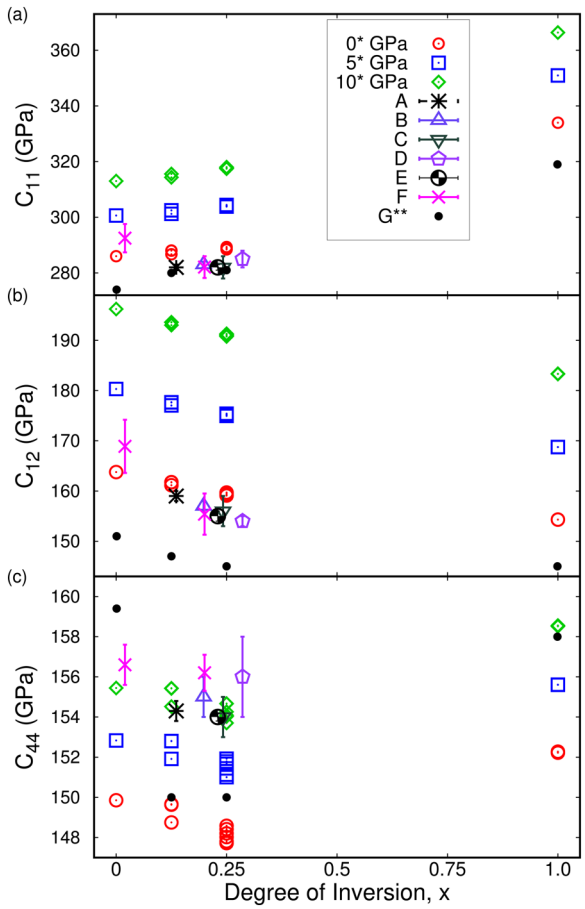

FIG. 2. Single crystal elastic constants (a) C_{11}, (b) C_{12}, and (c) C_{44} of $(Mg_{1-x}Al_x)[Mg_xAl_{2-x}]O_4$ spinel as a function of x. LDA results from this work at 0, 5, and 10 GPa are labeled by * and from Ref. 9 by G**. Experimental results are given by A: SP198B, B: sp3-600, C: sp3-800, D: sp-1050, E: Ref. 46, F: Ref. 16.

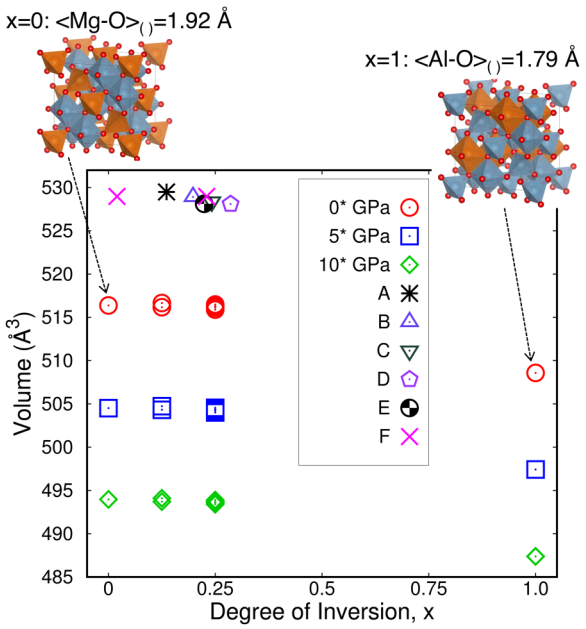

FIG. 3. Unit-cell volume of $(Mg_{1-x}Al_x)[Mg_xAl_{2-x}]O_4$ spinel as a function of x. The insets illustrate normal and inverse spinel to refer to the volume collapse for $x = 1$ at zero-pressure, as the average bond length $<Al\text{-}O>_{()}$, when tetrahedrally coordinated sites are filled by Al atoms, decreases in comparison to the case of normal spinel $<Mg\text{-}O>_{()}$. LDA results from this work at 0, 5, and 10 GPa are labeled by *. Experimental results are given by A: SP198B, B: sp3-600, C: sp3-800, D: sp3-1050, E: Ref. 46, F: Ref. 16.

of velocities and the direction cosines of their wave vectors were used to determine the 3 independent coefficients of the elastic tensor of each sample by least square fitting of the corresponding set of Christoffel's equations[43]

$$|C_{ijkl}n_jn_l - \rho v^2\delta_{ik}| = 0, \tag{4}$$

where C_{ijkl} are the elements of the elastic tensor (in full index notation), n_i are the wave vector direction cosines, ρ is the density, v is the acoustic velocity, and δ_{ik} is the Kronecker delta. The direction cosines of the acoustic wave vectors (n_1, n_2, n_3) were described by a set of Eulerian angles (θ, χ, ϕ) relating our experiment reference system to the crystal reference system. In our setup,[44] only the χ angle varies. This angle is the rotation around an axis oriented perpendicular to the faces of the sample platelet. Starting from an arbitrarily chosen direction (χ_0), the experimental rotation angle χ_i (i.e., the position of the Eulerian cradle goniometer) varies from 0 to 180° such that $\chi = \chi_0 + \chi_i$.[45] In our least square fitting procedure, we refined both the individual elastic tensor coefficients and the set of Eulerian angles, from which we could calculate the sample platelets' orientations. This was a check of consistency of our results because it confirmed the (111) orientation of our samples within 1°, compatible with the slight misorientations produced during the grinding and polishing procedures. One sample did not present well developed (111) faces, and it was polished in a general direction $(\bar{1}\ 0.7\ 1)$. Unit cell parameters, densities, oxygen fractional coordinates (here referred to the same setting as in Fig. 1), inversion degree, and the elastic tensor coefficients of the four samples are discussed in Sec. III. The samples' chemical formulas and bond lengths are tabulated in Table IV.

III. RESULTS AND DISCUSSION

A. $(Mg_{1-x}Al_x)[Mg_xAl_{2-x}]O_4$ spinel

To model and study the effects of inversion, x, on the structural and elastic properties of $(Mg_{1-x}Al_x)[Mg_xAl_{2-x}]O_4$, we first used SOD to find symmetrically inequivalent configurations for $x = 0.125, 0.25,$ and 1. The total number of configurations for each x in the conventional spinel unit-cell with $Z = 8$ is given by the number of combinations of Mg and Al atoms, n, to be inverted and distributed in the eight tetrahedrally and 16 octahedrally coordinated sites, r, i.e., $C(n, r) = n!/[r!(n - r)!]$. For example, two Mg atoms going into octahedra produce 120 configurations, while two Al atoms going into tetrahedra give 28 configurations, but from the total, only six of them are inequivalent for $x = 0.25$. However, on the extreme situation, inverse spinel with $x = 1$ is defined by 97 inequivalent configurations. For such a case, we only calculated the properties for a couple of inequivalent configurations. Although we acknowledge the shortcomings of our static calculations and the configurational method, we think that our work still gives reasonable insights on the effects of x on the elastic properties of Mg-Al spinel at

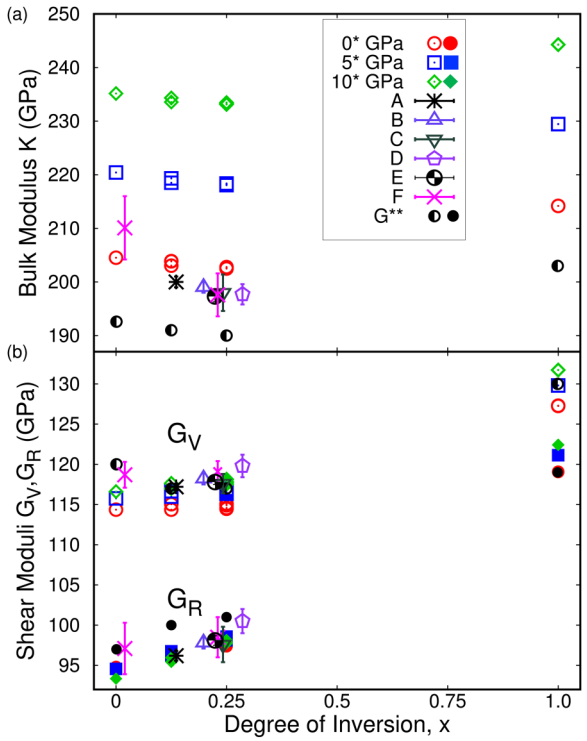

FIG. 4. $(Mg_{1-x}Al_x)[Mg_xAl_{2-x}]O_4$ spinel's (a) bulk (K) and (b) shear (G_V and G_R) moduli as a function of x at 0, 5, and 10 GPa. LDA results from this work are labeled by * and from Ref. 9 by G**. Experimental results are given by A: SP198B, B: sp3-600, C: sp3-800, D: sp-1050, E: Ref. 46, F: Ref. 16.

ambient and high-pressure. Temperature will likely affect the magnitude of structural and elastic properties, but the trends of the elastic coefficients related to the effect of inversion x will not be qualitatively modified as it was shown that the vibrational contribution to the free energy is virtually independent of x in a study of $(Co_{1-x}Al_x)[Co_xAl_{2-x}]O_4$.[47] Our investigations also go a step further, as earlier computational studies on spinel dealing explicitly with inversion only

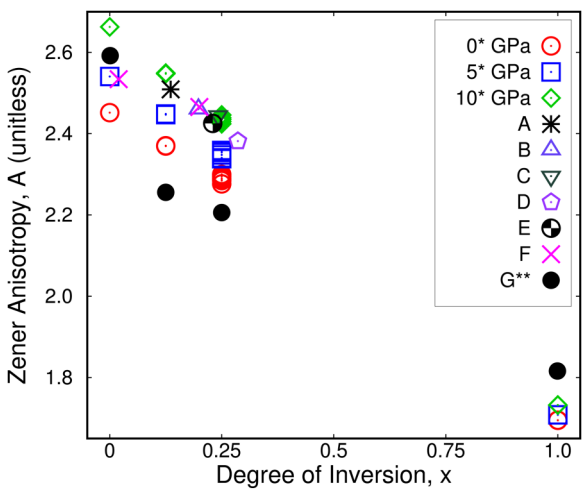

FIG. 5. Elastic anisotropy of $(Mg_{1-x}Al_x)[Mg_xAl_{2-x}]O_4$ spinel as a function of x. LDA results from this work at 0, 5, and 10 GPa are labeled by * and from Ref. 9 by G**. Experimental results are given by A: SP198B, B: sp3-600, C: sp3-800, D: sp-1050, E: Ref. 46, F: Ref. 16.

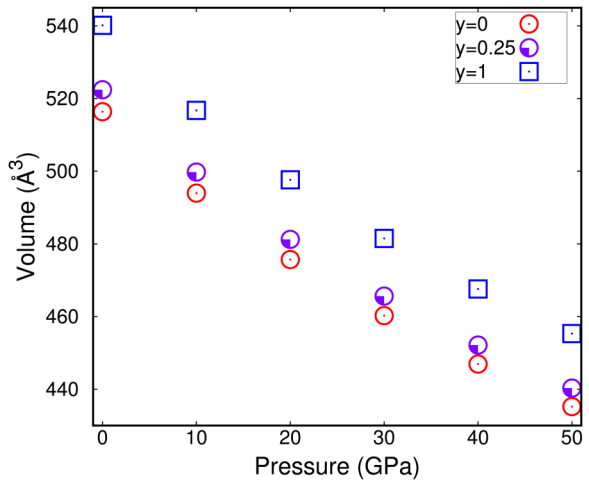

FIG. 6. LDA computed equation of state (EOS) for $MnAl_2O_4$ galaxite ($y = 1$) as a function of pressure compared to Mn-bearing ($y = 0.25$) and $MgAl_2O_4$ spinel ($y = 0$).

addressed its elastic properties at zero-pressure[9] (for $x = 0, 0.125, 0.25, 1$), greatly overestimated them (sometimes by more than 40% for $x = 0$)[13] or only showed some Raman spectra changes[12] (for $x = 0.2$).

We first computed the optimized ground-state crystal structure of normal spinel ($x = 0$) to obtain its elastic tensor C_{ij} within the GGA and LDA schemes. As it is well known, we notice that GGA overestimates the volume and, consequently, underestimates greatly the single crystal elastic

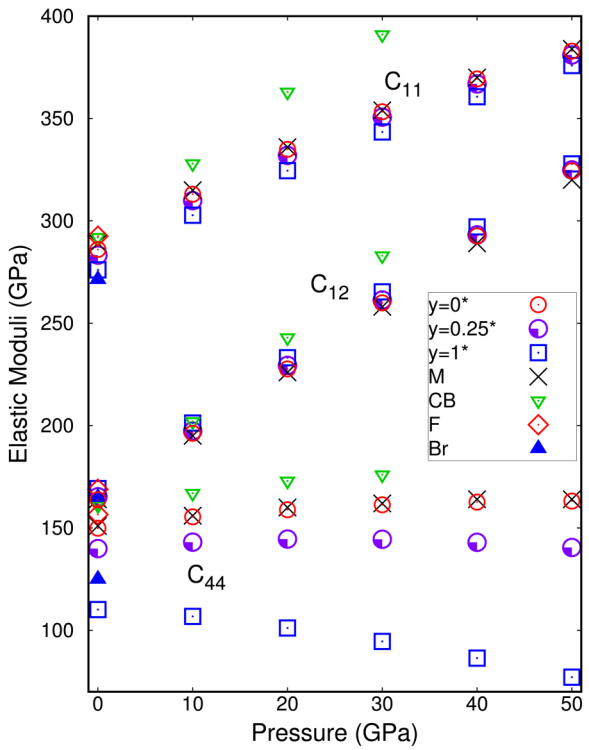

FIG. 7. Elastic tensor C_{ij} of $MnAl_2O_4$ galaxite ($y = 1$) as a function of pressure compared to Mn-bearing ($y = 0.25$) and $MgAl_2O_4$ spinel ($y = 0$). LDA results from this work are labeled by *. Other DFT results are given by CB: Ref. 12, M: Ref. 14. Experimental results are given by F: Ref. 16, Br: Ref. 18.

constants when compared to experimental results (see Table I). Thus, for the rest of our discussion and higher pressures, we only focus on LDA results. Our computations indicate that for normal spinel (Table I), while in absolute magnitude, our single crystal elastic constants deviate from experimental results[16] between ~2% and ~4%; our calculated trend is in agreement with the experimental one, i.e., $C_{11} >> C_{12} > C_{44}$ as also obtained in Refs. 12 and 14, but in contradiction with results from Ref. 9 in which $C_{11} >> C_{44} > C_{12}$.

The elastic tensor of $(Mg_{1-x}Al_x)[Mg_xAl_{2-x}]O_4$ spinel for $x = 0.125, 0.25,$ and 1 was obtained for a set of SOD-produced inequivalent configurations, which were also fully relaxed. Within this scheme, the conventional cubic unit-cell slightly distorts by $\lesssim$0.3% with respect to the lattice parameter and 90° angle for configurations with $0.125 \leq x < 1$ and between 0.7% and 1.3% for configurations with $x = 1$. However, as also previously reported,[9] here, we find that the ground-state energies obtained from full relaxations are lower (~8 meV/f.u.) than the energies from restricting the configurations to remain in the cubic unit-cell. Thus, we fully relaxed the $(Mg_{1-x}Al_x)[Mg_xAl_{2-x}]O_4$ structures having in mind that, in the bulk, the *collection* of all possible configurations deforming in different directions gives the experimental cubic symmetry reported for spinel. In Tables I and III, we give *average* unit-cell parameter a and *average* oxygen fractional coordinate u for all configurations with $x \neq 0$. Figure 2, and Tables I and III show our computed and experimental single crystal elastic constants of $(Mg_{1-x}Al_x)[Mg_xAl_{2-x}]O_4$ spinel for $x = 0, 0.125, 0.25,$ and 1. As we can observe, at zero pressure, our computed C_{11} [Fig. 2(a)] and C_{12} [Fig. 2(b)] elastic constants for $x = 0.125$ and $x = 0.25$ are in very good agreement with our experimental results near that range, with C_{11} increasing and C_{12} decreasing as x increases. However, while the experimental trend given by our Brillouin measurements and other experimental results is well reproduced by our calculated C_{44} progression as a function of x [Fig. 2(c)], first slightly decreasing for x between 0 and 0.25 and then increasing, the experimental magnitudes appear larger than the LDA results. This apparent dissimilarity is somewhat puzzling considering that our predicted C_{11} and C_{12} are very consistent with our measurements. Additionally, as pressure increases, we predict that the ambient pressure behavior of C_{ij} prevails up to 10 GPa.

Figure 3 shows how the spinel's volume changes as a function of x and pressure. From our simulations, we notice that as x changes from 0 to 1, there is a drop in the volume of inverse spinel of almost 2%. This volume reduction can be explained due to the fact that at $x = 1$, all Mg atoms in tetrahedra have been exchanged for Al atoms in octahedra and as a result, their ionic radius (in Å) changes[40] ($r_{Mg^{2+}_{()}}$ ~0.586→ $r_{Mg^{2+}_{[]}}$ ~0.702 and $r_{Al^{3+}_{[]}}$ ~0.528→ $r_{Al^{3+}_{()}}$ ~0.394), and, for example, at zero-pressure the average cation-oxygen bond length in tetrahedra (<Mg-O>$_{()}$→<Al-O>$_{()}$) decreases by about 7% (in line with the experimentally observed decrease of about 3% when $x = 0.18$ goes to $x = 0.29$[34]). Using our computed single crystal elastic constants, we obtain the aggregate bulk (K) and shear (G_V, G_R) moduli calculated within the Voigt-Reuss scheme,[48] which for cubic symmetry are given by

$$K_V = K_R = \frac{C_{11} + 2C_{12}}{3} = K, \tag{5}$$

$$\begin{aligned} G_V &= \frac{C_{11} - C_{12} + 3C_{44}}{5}, \\ G_R &= \frac{5(C_{11} - C_{12})C_{44}}{3(C_{11} - C_{12}) + 4C_{44}}. \end{aligned} \tag{6}$$

Predicted K, G_V, and G_R are shown and compared with our measurements and other DFT and experimental results in Fig. 4 as a function of x for different pressures. One can see that as x increases between 0 and 0.25, the bulk modulus decreases, Fig. 4(a), but at $x = 1$, inverse spinel's K becomes stiffer than that of normal spinel. In contrast, Mg-Al spinel's G_R steadily increases with x between 0 and 1, while G_V remains somewhat constant for small x, Fig. 4(b). Upon increasing pressure, $K(x)$ remarkably increases in magnitude for all x, while $G_V(x)$ and $G_R(x)$ only slightly change with respect to ambient pressure values, particularly for $x < 0.25$.

Finally, the fact that spinel is a very anisotropic material is reflected in the large difference between G_V and G_R [see Fig. 4(b)]. Figure 5 shows the change in the elastic anisotropy A, Eq. (1), for Mg-Al spinel as a function of x and pressure. First, we notice that spinel becomes more anisotropic as pressure increases independently of its degree of inversion, though the effect is more evident for $x < 0.25$. Second, as the degree of inversion, x, increases, Mg-Al spinel

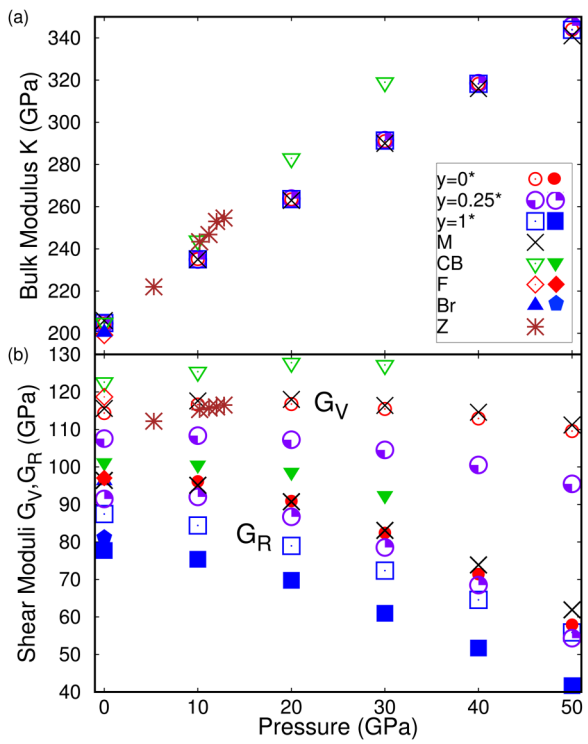

FIG. 8. Aggregate properties of $MnAl_2O_4$ galaxite ($y = 1$) as a function of pressure compared to Mn-bearing ($y = 0.25$) and $MgAl_2O_4$ spinel ($y = 0$). LDA results from this work are labeled by *. DFT results are given by CB: Ref. 12 and M: Ref. 14. Experimental results are given by F: Ref. 16, Br: Ref. 18, and Z: Ref. 50.

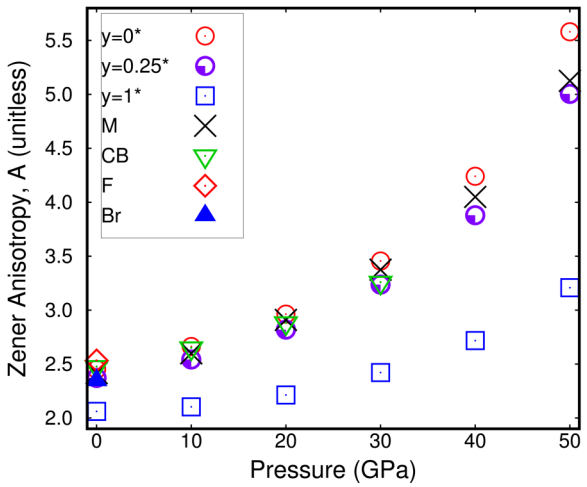

FIG. 9. Elastic anisotropy of $MnAl_2O_4$ galaxite ($y = 1$) as a function of pressure compared to Mn-bearing ($y = 0.25$) and $MgAl_2O_4$ spinel ($y = 0$). LDA results from this work are labeled by *. DFT results are given by CB: Ref. 12, M: Ref. 14. Experimental results are given by F: Ref. 16 and Br: Ref. 18.

significantly tends to be less anisotropic ($A = 1$ implies an elastically isotropic cubic crystal), with A reducing by about 30% for inverse spinel with respect to normal spinel. We attribute this large decrease of A to the stiffening of the tetrahedra due to the different cation size of Mg and Al, which controls the shear modulus, $(C_{11} - C_{12})/2$, along $\langle 110 \rangle$ directions. This tendency toward isotropy is also seen in the closer magnitudes of $G_V(x = 1)$ and $G_R(x = 1)$. This feature of spinel, e.g., would explain in part its outstanding capabilities to withstand radiation and be used as a shielding material. As the atomic structure of Mg-Al spinel undergoes energetic collisions caused, for instance, by neutron radiation, the spinel structure would cope with it by *rearranging* its atoms through the cation inversion mechanism[49] in order to maintain its original symmetry and elastic properties, especially for a moderate degree of inversion. The effect of cation inversion on the elastic anisotropy of $MgAl_2O_4$ is qualitatively opposite to that determined for ringwoodite (Mg_2SiO_4) in two first-principles studies[9,8] that show 5% to 11% increase of A when x changes from 0 to 0.125. These results

TABLE II. Unit-cell parameter a (Å), oxygen fractional coordinate u, density ρ (kg/m^3), elastic tensor C_{ij} (GPa), bulk modulus K (GPa), and shear moduli G_V and G_R (GPa) of $(Mg_{1-y}Mn_y)Al_2O_4$ spinel-galaxite as a function of y and pressure P (GPa). Results from this work are labeled by *.

P	y	a	u	ρ	C_{11}	C_{12}	C_{44}	K	G_V	G_R	Ref.
0	0	8.02	0.3883	3659.76	286.01	163.77	149.85	204.52	114.36	94.80	LDA*
		—	—		292	162	161	193	123	101	LDA[a]
		—	—	3650	289	164	151	206	116	96	LDA[b]
10		7.90	0.3879	3825.79	313.00	196.24	155.44	235.16	116.62	93.35	LDA*
		—	—		328	202	167	244	125	101	LDA[a]
		—	—	3800	315	195	156	235	118	95	LDA[b]
20		7.81	0.3875	3972.89	334.93	227.70	158.88	263.45	116.77	88.99	LDA*
		—	—		363	243	173	283	128	99	LDA[a]
		—	—	3950	336	226	160	263	118	91	LDA[b]
30		7.72	0.3871	4106.09	353.30	259.92	161.31	291.05	115.46	81.39	LDA*
		—	—		391	283	176	319	127	92	LDA[a]
		—	—	4080	354	258	162	290	116	83	LDA[b]
40		7.65	0.3869	4228.56	369.34	292.64	162.64	318.21	112.92	70.82	LDA*
		—	—	4190	370	289	164	316	115	74	LDA[b]
50		7.58	0.3866	4342.23	382.93	324.47	163.12	343.95	109.56	57.59	LDA*
		—	—	4310	384	320	164	341	111	62	LDA[b]
0	0.25	8.05	0.3921	3812.23	283.24	165.21	139.93	204.55	107.56	90.37	LDA*
10		7.94	0.3917	3985.08	309.87	197.32	143.06	234.84	108.35	88.48	LDA*
20		7.84	0.3914	4138.36	331.96	229.40	144.56	263.58	107.25	83.68	LDA*
30		7.75	0.3912	4277.18	350.63	261.36	144.47	291.12	104.54	76.25	LDA*
40		7.68	0.3909	4404.70	366.87	293.16	142.99	317.73	100.54	66.45	LDA*
50		7.61	0.3907	4523.14	381.04	324.91	140.44	343.62	95.49	53.98	LDA*
0	1	8.14	0.3913	4252.10	276.06	169.22	110.12	204.83	87.44	77.30	LDA*
		8.28	0.3913	4041	248.31	148.02	108.01	181.45	84.87	73.90	GGA[c]
		8.21	0.3909	4150	271.3(1.3)	164.8(1.3)	124.9(0.5)	200.3(1.0)	96.2(5)	81.2(5)	EXP[d,e]
10		8.02	0.3910	4444.90	302.76	201.23	106.80	235.07	84.39	74.09	LDA*
20		7.92	0.3907	4615.59	324.52	233.15	101.12	263.60	78.95	68.08	LDA*
30		7.84	0.3905	4770.21	343.43	265.33	94.56	291.36	72.36	60.28	LDA*
40		7.76	0.3903	4912.12	360.64	297.06	86.40	318.25	64.56	51.21	LDA*
50		7.69	0.3901	5044.49	375.89	327.81	77.11	343.84	55.88	40.95	LDA*

[a]Reference 12.
[b]Reference 14.
[c]Reference 33.
[d]Reference 18.
[e]Reference 51.

indicate that the effects of inversion on spinel oxides' properties strongly depend on the nature of the involved cations.

B. $(Mg_{1-y}Mn_y)Al_2O_4$ spinel-galaxite

In order to investigate the elastic anisotropy behavior at high pressure of the Mn-Al spinel end member, galaxite, first we obtained the static zero-pressure optimized structure with antiferromagnetic (AFM) ordering, as this configuration was lower in energy than the structure with ferromagnetic (FM) ordering by ~22 meV/f.u. Figure 6 shows our computed equation of state (EOS), i.e., unit-cell volume as a function of pressure, for $MnAl_2O_4$ in comparison to that of $MgAl_2O_4$ and $(Mg_{0.75}Mn_{0.25})Al_2O_4$. We can observe that upon Mn substitution, Mn→Mg, there is a volume expansion due to the larger Mn^{2+} ionic radius.[52] The elastic tensor of $MnAl_2O_4$ galaxite as a function of pressure is shown in Fig. 7 and Table II, and it is contrasted with the elastic moduli of $MgAl_2O_4$ spinel. The most significant change in magnitude can be seen in the C_{44} elastic constant upon Mn→Mg. For $MgAl_2O_4$, C_{44} slightly increases with pressure between 0 and 50 GPa, but once that Mn starts substituting Mg, C_{44} notably decreases with increasing pressure as it is clearly seen for $MnAl_2O_4$. On the other hand, C_{11} and C_{12} are barely affected by the Mn→Mg substitution, and they both strongly increase with pressure. Looking at the tetragonal shear modulus given by $(C_{11} - C_{12})/2$, as pressure increases it decreases for both spinel and galaxite, and for the latter it vanishes first than C_{44}. The significant softening of $(C_{11} - C_{12})/2$ with increasing hydrostatic pressure is generally a precursory phenomenon related to crystal structure transformation and it is common to both $MgAl_2O_4$ and $MnAl_2O_4$. Hence, the strong decrease of C_{44} for the latter is not indicating by itself that galaxite is more mechanically unstable. It is also noted that elastic properties' measurements of $MnAl_2O_4$ are very limited, but our C_{ij} at zero pressure are in good agreement with available experimental findings.[18] Our computed aggregate elastic moduli (K, G_V, and G_R) as a function of pressure for $MnAl_2O_4$, Mn-bearing spinel, and $MgAl_2O_4$ are shown in Fig. 8 and Table II. Our calculations, contrasted to previous *ab initio* and experimental results[12,14,50] for $MgAl_2O_4$, indicate that galaxite's bulk modulus [see Fig. 8(a)] is very similar in magnitude to spinel's K, with both increasing almost linearly with pressure. The shear moduli of galaxite [see Fig. 8(b)], on the other hand, are noticeably smaller than their counterparts for spinel and with increasing pressure, they decrease at a faster rate. Finally, Fig. 9 shows our predicted Zener anisotropy of galaxite, and we can observe that as Mg starts being replaced by Mn in the spinel structure, the elastic anisotropy A decreases and even though, A increases with pressure for both galaxite and spinel, for the latter it happens more rapidly.

At ambient conditions, galaxite is less anisotropic than normal spinel; this behavior has also been reported for $CoAl_2O_4$.[53] The origin of the decrease of A from normal $MgAl_2O_4$ to $MnAl_2O_4$ and $CoAl_2O_4$ is that the magnetic (Co,Mn)→Mg substitutions in tetrahedra weaken the rigidity C_{44} along ⟨100⟩ much more effectively than that along the ⟨110⟩ directions. One could naively assign this decrease of A to geometric effects. For instance, considering the sequence of ionic radii (in Å) for different transition metals in tetrahedral coordination[40] with respect to Mg^{2+}, $r_{Mg^{2+}} \sim 0.586 < r_{Co^{2+}} \sim 0.592 < r_{Fe^{2+}} \sim 0.620 < r_{Mn^{2+}} \sim 0.656$, one would expect to see a decrease of anisotropy for $FeAl_2O_4$ as well; yet, it has been observed that its anisotropy increases.[54] This unexpected behavior of A for Fe→Mg substitution is also consistent with experimental results for intermediate compositions.[55] Thus, we discard the cation size as the cause of the decrease in A by transition metal substitution and attribute more the elastic anisotropy behavior[53,54] ($A_{Co} = 2.31 < A_{Mn} = 2.34 < A_{Mg} = 2.44 < A_{Fe} = 3.20$) to the crystal field stabilization of the magnetic cation occupying the tetrahedral site, Mn in the case of our work. Analyzing the tetrahedral crystal field splitting (spin occupancy of the e and t_2 energy levels) of Mn^{2+} (e^2, t_2^3), Fe^{2+} (e^3, t_2^3), and Co^{2+} (e^4, t_2^3), the "odd" behavior of A for $FeAl_2O_4$ has its origin in the uneven occupation of its e energy levels. In essence, there is a stronger correlation between the spin configuration of the cation in the tetrahedral site and the elastic anisotropy than between cation size and A for normal MAl_2O_4 spinel end-members with M = Mg, Co, Mn, Fe.

IV. SUMMARY AND CONCLUSIONS

Using first-principles calculations and Brillouin scattering, we obtained the elastic tensor, C_{ij}, and aggregate elastic moduli, K, G_V, and G_R, of $(Mg_{1-x}Al_x)[Mg_xAl_{2-x}]$ spinel for various degrees of inversion ($0 < x \leq 1$), additionally, and to the best of our knowledge for the first time, we showed the high-pressure behavior of the single crystal elastic constants for $MnAl_2O_4$ galaxite. Overall, our computational and experimental findings are consistent with each other and follow the relationship $C_{11} >> C_{12} > C_{44}$ for all degrees of inversion and pressures considered in this study of $(Mg_{1-x}Al_x)[Mg_xAl_{2-x}]$ spinel. Major discrepancies between our experimental and computational results could be attributed to our calculations being performed at zero Kelvin and the limited sampling of configurations for $x \neq 0, 0.25$; nevertheless, we think that our investigations give clearer results to better understand the measured elastic properties for Mg-Al spinels with different degrees of inversion than previous studies.[9,12,13] We have also demonstrated that increasing inversion, x, in spinel lowers its elastic anisotropy and that magnetic substitution at the tetrahedrally coordinated sites, Mn→Mg, has a similar effect in the elastic anisotropy, that is, galaxite and inverse spinel are about 16% and 30% less anisotropic than $MgAl_2O_4$, respectively. This behavior is the opposite of that of ringwoodite (Mg_2SiO_4) which shows a ~10% increase of A for $x = 0.125$.

ACKNOWLEDGMENTS

M.N.V. gratefully acknowledges the computing time granted by the John von Neumann Institute for Computing (NIC) and provided on the supercomputer JURECA at Jülich Supercomputing Centre (JSC) under project ID HPO24. M.N.V. is supported by the W2-Professorship Funding from the Helmholtz Association.

APPENDIX: ADDITIONAL MODELING AND EXPERIMENTAL RESULTS

In the following two tables, we summarize the high pressure results for $(Mg_{1-x}Al_x)[Mg_xAl_{2-x}]O_4$ spinel (Table III) and the ambient pressure experimental average octahedral and tetrahedral bond lengths of the samples investigated in this work (Table IV).

TABLE III. High pressure P (GPa), unit-cell parameter a (Å), oxygen fractional coordinate u, density ρ (kg/m^3), elastic tensor C_{ij} (GPa), bulk modulus K (GPa), and shear moduli G_V and G_R (GPa) of $(Mg_{1-x}Al_x)[Mg_xAl_{2-x}]O_4$ spinel with different degrees of inversion x. Results from this work are labeled by *.

P	x	a	u	ρ	C_{11}	C_{12}	C_{44}	K	G_V	G_R	Ref.
5	0	7.961	0.38808	3745.86	300.63	180.32	152.83	220.42	115.76	94.56	LDA*
	0.125	7.960	0.38665	3747.28	302.49	177.65	152.80	219.38	116.65	96.76	LDA*
		7.962	0.38468	3744.16	301.22	177.05	151.91	218.55	115.98	96.23	LDA*
		7.960	0.38500	3747.28	302.50	177.69	152.80	219.37	116.64	96.75	LDA*
	0.25	7.960	0.38480	3747.65	303.83	175.14	151.79	218.37	116.81	98.34	LDA*
		7.961	0.38468	3745.57	304.04	175.40	151.01	218.27	116.33	98.11	LDA*
		7.960	0.38324	3746.91	304.37	174.96	151.44	218.09	116.75	98.58	LDA*
		7.959	0.38519	3748.02	304.44	175.34	151.92	218.37	116.97	98.56	LDA*
		7.960	0.38683	3746.91	303.91	175.21	151.67	218.11	116.74	98.31	LDA*
		7.958	0.38644	3748.02	304.23	174.97	151.13	218.06	116.53	98.43	LDA*
	1	7.923	0.37991	3799.26	350.94	168.76	155.60	229.43	129.80	121.25	LDA*
		7.923	0.37940	3799.26	350.93	168.74	155.61	229.40	129.81	121.26	LDA*
10	0	7.905	0.38785	3825.79	313.00	196.24	155.44	235.16	116.62	93.35	LDA*
		—	—	—	328	202	167	244	125	101	LDA[a]
		—	—	—	315	195	156	235	118	95	LDA[b]
	0.125	7.906	0.38457	3824.79	314.34	193.03	154.52	233.56	116.98	95.44	LDA*
		7.904	0.38644	3827.81	316.12	193.64	156.24	234.33	117.64	95.96	LDA*
		7.904	0.38484	3827.81	316.10	193.58	155.03	234.34	117.65	95.97	LDA*
	0.25	7.905	0.38451	3826.41	318.30	192.05	157.05	233.47	118.09	97.99	LDA*
		7.903	0.38473	3828.50	319.17	191.89	156.04	233.33	117.52	97.78	LDA*
		7.903	0.38311	3827.73	319.91	190.69	154.27	233.16	117.88	98.17	LDA*
		7.961	0.38502	3828.82	318.07	192.23	157.35	233.46	118.17	98.17	LDA*
		7.904	0.38664	3827.81	317.45	190.93	154.03	233.10	117.72	97.86	LDA*
		7.902	0.38632	3828.82	317.45	191.32	154.26	233.36	117.78	97.73	LDA*
	1	7.870	0.37991	3877.44	373.30	184.63	158.32	244.25	131.74	122.63	LDA*
		7.870	0.37940	3877.60	373.41	184.66	158.25	244.30	131.71	122.61	LDA*

[a]Reference 12.
[b]Reference 14.

TABLE IV. Structural formula, average octahedral bond distance <M-O> (Å), and average tetrahedral bond distance <T-O> (Å) of the spinels experimentally (EXP) investigated in this study. A: SP198B, B: sp3-600, C: sp3-800, D: sp3-1050. Experimental 1σ uncertainties on the last digits are reported in parentheses. The results from Ref. 46 are included at the end of the table.

Formula	<M-O>	<T-O>	Ref.
$(Mg_{0.852}Al_{0.136}Fe_{0.008}Zn_{0.004})$ $[Mg_{0.163}Al_{1.820}Cr_{0.013}V_{0.003}]O_4$	1.92043(19)	1.9389(4)	EXP A
$(Mg_{0.802}Al_{0.198})[Mg_{0.198}Al_{1.802}]O_4$	1.9250(2)	1.9280(5)	EXP B
$(Mg_{0.758}Al_{0.242})[Mg_{0.242}Al_{1.758}]O_4$	1.9283(3)	1.9197(7)	EXP C
$(Mg_{0.714}Al_{0.286})[Mg_{0.286}Al_{1.714}]O_4$	1.9320(3)	1.9116(6)	EXP D
$(Mg_{0.776}Al_{0.224})[Mg_{0.224}Al_{1.776}]O_4$	1.92640(3)	1.9224(6)	[a]

[a]Reference 46.

[1]I. Ganesh, "A review on magnesium aluminate ($MgAl_2O_4$) spinel: Synthesis, processing and applications," Int. Mater. Rev. **58**, 63–112 (2013).
[2]R. J. Bratton, "Translucent sintered ($MgAl_2O_4$)," J. Am. Ceram. Soc. **57**, 283 (1974).
[3]V. T. Gritsyna, Y. G. Kazarinov, V. A. Kobyakov, and I. E. Reimanis, "Radiation-induced luminescence in magnesium aluminate spinel crystals and ceramics," Nucl. Instrum. Methods Phys. Res. Sect. B **250**, 342–348 (2006).
[4]H. Yoshida, P. Biswas, R. Johnson, and M. K. Mohan, "Flash-sintering of magnesium aluminate spinel ($MgAl_2O_4$) ceramics," J. Am. Ceram. Soc. **100**, 554–562 (2017).
[5]K. Momma and F. Izumi, "Vesta: A three dimensional visualization system for electronic and structural analysis," J. Appl. Cryst. **41**, 653–658 (2008).
[6]C. Zener, *Elasticity and Anelasticity of Metals* (University of Chicago Press, 1948), p. 170.
[7]W. L. Griffin, J. C. Afonso, E. A. Belousova, S. E. Gain, X.-H. Gong, J. González-Jiménez, D. Howell, J.-X. Huang, N. McGowan, N. Pearson, T. Satsukawa, R. Shi, P. Williams, Q. Xiong, J.-S. Yang, M. Zhang, and S. O'Reilly, "Mantle recycling: Transition zone metamorphism of tibetan ophiolitic peridotites and its tectonic implications," J. Petrol. **57**, 655–684 (2016).
[8]W. Panero, "Cation disorder in ringwoodite and its effects on wave speeds in the earth's transition zone," J. Geophys. Res. **113**, B10204 (2008).
[9]L. Li, P. Carrez, and D. Weidner, "Effect of cation ordering and pressure on spinel elasticity by ab initio simulation," Am. Mineral. **92**, 174–178 (2007).
[10]P. Hohenberg and W. Kohn, "Inhomogeneous electron gas," Phys. Rev. B **136**, 864–871 (1964).
[11]W. Kohn and L. J. Sham, "Self-consistent equations including exchange and correlation effects," Phys. Rev. A **140**, 1133–1138 (1964).

[12]R. Caracas and E. J. Banigan, "Elasticity and Raman and infrared spectra of $MgAl_2O_4$ spinel from density perturbation theory," Phys. Earth Planet. Inter. **174**, 113–121 (2009).
[13]P. Shukla, A. Chernatynskiy, J. C. Nino, S. B. Sinnott, and S. R. Phillpot, "Effect of inversion on thermoelastic and thermal transport properties of $MgAl_2O_4$ spinel by atomistic simulation," J. Mater. Sci. **46**, 55–62 (2011).
[14]X.-C. Mao, K. Liu, B.-S. Hou, J. Tan, and X.-L. Zhou, "Theoretical investigation of the structural, elastic, and thermodynamic properties of $MgAl_2O_4$ spinel under high pressure," J. Phys. Soc. Jpn. **85**, 114605 (2016).
[15]Z. P. Chang and G. R. Barsch, "Pressure dependence of single-crystal elastic constants and anharmonic properties of spinel," J. Geophys. Res. **78** (14), 2418–2433 (1973).
[16]H. Cynn, O. L. Anderson, and M. Nicol, "Effects of cation disordering in a natural $MgAl_2O_4$ spinel observed by rectangular parallelepiped ultrasonic resonance and Raman measurements," Pure Appl. Gephys. Res. Lett. **141**, 415–444 (1993).
[17]I. Susuki, I. Ohno, O. L. Anderson, R. C. E.Liebermann, and D. G. E. Isaak, "Harmonic and anharmonic properties of spinel $MgAl_2O_4$," Am. Mineral. **85**, 304–311 (2000).
[18]E. Bruschini, S. Speziale, G. B. Andreozzi, F. Bosi, and U. Hålenius, "The elasticity of $MgAl_2O_4$-$MnAl_2O_4$ spinels by Brillouin scattering and an empirical approach for bulk modulus prediction," Am. Mineral. **100**, 644 (2015).
[19]P. E. Blöchl, "Projector augmented-wave method," Phys. Rev. B **50**, 17953 (1994).
[20]G. Kresse and J. Hafner, "Ab initio molecular dynamics for liquid metals," Phys. Rev. B **47**, 558 (1993).
[21]G. Kresse and J. Hafner, "Ab initio molecular-dynamics simulation of the liquid-metal-amorphous-semiconductor transition in germanium," Phys. Rev. B **49**, 14251 (1994).
[22]G. Kresse and J. Furthmüller, "Efficiency of ab-initio total energy calculations for metals and semiconductors using a plane-wave basis set," Comp. Mater. Sci. **6**, 15 (1996).
[23]G. Kresse and J. Furthmüller, "Efficient iterative schemes for ab initio total-energy calculations using a plane-wave basis," Phys. Rev. B **54**, 11169 (1996).
[24]Jülich Supercomputing Centre, "General-purpose supercomputer at Jülich supercomputing centre," J. Large-scale Res. Facil. **2**, A62 (2016).
[25]D. M. Ceperley and B. J. Alder, "Ground state of the electron gas by a stochastic method," Phys. Rev. Lett. **45**, 566 (1980).
[26]J. P. Perdew, K. Burke, and M. Ernzerhof, "Generalized gradient approximation made simple," Phys. Rev. Lett. **77**, 3865–3868 (1996).
[27]Y. L. Page and P. Saxe, "Symmetry-general least-squares extraction of elastic data for strained materials from ab initio calculations of stress," Phys. Rev. B **65**, 104104 (2002).
[28]R. Grau-Crespo, C. R. A. Catlow, and N. H. d. Leeuw, "Symmetry-adapted configurational modelling of fractional site occupancy in solids," J. Phys. Condens. Matter **19**, 256201 (2007).
[29]S. L. Dudarev, G. A. Botton, S. Y. Savrasov, C. J. Humphreys, and A. P. Sutton, "Electron-energy-loss spectra and the structural stability of nickel oxide: An LSDA+U study," Phys. Rev. B **57**, 1505 (1998).
[30]V. L. Campo and M. Cococcioni, "Extended DFT + U + V method with on-site and inter-site electronic interactions," J. Phys.: Condens. Matter **22**, 055602 (2010).
[31]U. Aschauer, N. Vonrüti, and N. A. Spaldin, "Effect of epitaxial strain on cation and anion vacancy formation in MnO," Phys. Rev. B **92**, 054103 (2015).
[32]D. Santos-Carballal, P. E. Ngoepe, and N. H. de Leeuw de, "*Ab initio* investigation of the thermodynamics of cation distribution and of the electronic and magnetic structures in the $LiMn_2O_4$ spinel," Phys. Rev. B **97**, 085126 (2018).
[33]S. Akbudak, A. Kushwaha, G. Ugur, S. Ugur, and H. Y. Ocak, "Structural, electronic, elastic, optical and vibrational properties of MAl_2O_4 (M = Co and Mn) aluminate spinels," Ceram. Int. **44**, 310–316 (2018).
[34]G. B. Andreozzi, F. Princivalle, H. Skogby, and A. Della Giusta, "Cation ordering and structural variations with temperature in $MgAl_2O_4$ spinel: An x-ray single-crystal study," Am. Mineral. **85**, 1164–1171 (2000).
[35]G. B. Andreozzi and F. Princivalle, "Kinetics of cation ordering in synthetic $MgAl_2O_4$ spinel," Am. Mineral. **87**, 838–844 (2002).
[36]R. A. Fregola, N. Melone, and E. Scandale, "X-ray diffraction topographic study of twinning and growth of natural spinels," Eur. J. Mineral. **17**, 761–768 (2005).
[37]F. Bosi, H. Skogby, R. A. Fregola, and U. Hålenius, "Crystal chemistry of spinels in the system $MgAl_2O_4$-MgV_2O_4-Mg_2VO_4," Am. Mineral. **101**, 580–586 (2016).
[38]G. Sheldrick, *Shelxl-97. Program for Solution and Refinement of Crystal Structures* (Institut Anorganische Chemie, Göttingen, 1997).
[39]F. Bosi, U. Hålenius, and H. Skogby, "Crystal chemistry of the $MgAl_2O_4$-$MgMn_2O_4$-$MnMn_2O_4$ system: Analysis of structural distortion in spinel- and hausmannite-type structures," Am. Mineral. **95**, 602–607 (2010).
[40]B. Lavina, G. Salviulo, and A. Della Giusta, "Cation distribution and structure modelling of spinel solid solutions," Phys. Chem. Minerals **29**, 10–18 (2002).
[41]C. Whitfield, E. Brody, and W. Bassett, "Elastic moduli of NaCl by brillouin scattering at high pressure in a diamond anvil cell," Rev. Sci. Instrum. **47** (8), 942–947 (1976).
[42]J. Sandercock, "Trends in brillouin scattering: Studies of opaque materials, supported films, and central modes," in *Topics in Applied Physics*, edited by M. Cardona and G. Guntherodt (Springer Verlag, Berlin, 1982), Vol. 51, p. 173.
[43]M. Musgrave, *Crystal Acoustics: Introduction to the Study of Elastic Waves and Vibrations in Crystals* (Holden-Day, 1970), p. 288.
[44]S. Speziale and T. Duffy, "Single-crystal elastic constants of fluorite (CaF_2) to 9.3 GPa," Phys. Chem. Minerals **29**, 465–472 (2002).
[45]F. Jiang, S. Speziale, S. Shieh, and T. Duffy, "Single-crystal elasticity of andradite to 11 GPa," J. Phys.: Condens. Matter **16**, S1041–S1052 (2004).
[46]S. Speziale, F. Nestola, F. Jiang, and T. Duffy, "Single crystal elastic constants of spinel ($MgAl_2O_4$) to 11.1 GPa by brillouin scattering," Abstract MR23A-2658, AGU Fall Meeting, 2016.
[47]F. Tielens, M. Calatayud, R. Franco, J. M. Recio, J. Pérez-Ramírez, and C. Minot, "Periodic DFT study of the structural and electronic properties of bulk $CoAl_2O_4$ spinel," J. Phys. Chem. B **110**, 988–995 (2006).
[48]R. Hill, Proc. Phys. Soc. London **65**, 349 (1952).
[49]K. Sickafus, A. Larson, N. Yu, M. Nastasi, G. Hollenberg, F. Garner, and R. Bradt, "Cation disorder in high dose, neutron-irradiated spinel," J. Nucl. Mater. **219**, 128–134 (1995).
[50]Y. Zou, S. Gréaix, T. Irifune, B. Li, and Y. Hugo, "Unusual pressure effect on the shear modulus in $MgAl_2O_4$ spinel," J. Phys. Chem. C **117**, 24518–24526 (2013).
[51]U. Hålenius, F. Bosi, and S. H, "Galaxite, $MnAl_2O_4$, a spectroscopic standard for tetrahedrally coordinated Mn^{2+} in oxygen-based mineral structures," Am. Mineral. **92**, 1225–1231 (2007).
[52]R. D. Shannon and C. T. Prewitt, "Effective ionic radii in oxides and fluorides," Acta Crystallogr. B **25**, 925 (1969).
[53]Z. Li, E. S. Fisher, J. Z. Liu, and M. V. Nevitt, "Single-crystal elastic constants of Co-AI and Co-Fe spinels," J. Mater. Sci. **26**, 2621–2624 (1991).
[54]H. Wang and G. Simmons, "Elasticity of some mantle crystal structures. I. Pleonaste and hercynite spinel," J. Geophys. Res. **77**, 4380–4392 (1972).
[55]E. Bruschini, S. Speziale, F. Bosi, and G. B. Andreozzi, "Fe-Mg substitution in aluminate spinels: Effects on elastic properties investigated by brillouin scattering," Phys. Chem. Minerals **45**, 759–772 (2018).